A CPT-based multi-spring model for lateral monopile analysis under SLS conditions in sand

Tott-Buswell, Jacques; Prendergast, Luke J.; Gavin, Kenneth

DOI
10.1016/j.oceaneng.2023.116642

Publication date
2024

Document Version
Final published version

Published in
Ocean Engineering

Citation (APA)
Tott-Buswell, J., Prendergast, L. J., & Gavin, K. (2024). A CPT-based multi-spring model for lateral monopile analysis under SLS conditions in sand. *Ocean Engineering*, *293*, Article 116642. https://doi.org/10.1016/j.oceaneng.2023.116642

Ocean Engineering 293 (2024) 116642

Contents lists available at ScienceDirect

Ocean Engineering

journal homepage: www.elsevier.com/locate/oceaneng

A CPT-based multi-spring model for lateral monopile analysis under SLS conditions in sand

Jacques Tott-Buswell [a,*], Luke J. Prendergast [a], Kenneth Gavin [b]

[a] University of Nottingham, Department of Civil Engineering, Nottingham, NG7 2RD, United Kingdom
[b] Delft University of Technology, Faculty of Civil Engineering and Geosciences, Delft, 2628 CN, The Netherlands

ARTICLE INFO

Keywords:
In-situ testing
Numerical modelling
Offshore engineering
Piles & piling
Soil–structure interaction

ABSTRACT

Monopiles are the most common Offshore Wind Turbine (OWT) foundations due to their simplicity in design, fabrication, and installation. However, large new-generation turbines have led to significant changes in monopile dimensions, necessitating extensive finite element analyses and ground investigations to meet design requirements. While Cone Penetration Test (CPT)-based p-y methods can analyse slender pile lateral behaviour, they often miss additional resistance mechanisms relevant to rigid monopiles. This paper introduces CPT-informed resistance mechanisms for monopiles to incorporate additional lateral resistances beyond p-y modelling capabilities. Distributed moment–rotation (m-θ) springs are defined by repurposing CPT-based axial capacity estimation methods for piles; and pile tip shear and moment springs are informed by approximating a residual bearing stress post-installation using local CPT q_c values. The performance of the multi-spring model is appraised against data reported from monotonic pile pushover tests conducted at two sand sites. Results show that the multi-spring model is capable of predicting pile head deflections reasonably well within serviceability deflection limits against the reported test data, but ultimate failure loads cannot be predicted using the proposed model. A clear sensitivity in pile response to local variations in CPT q_c is demonstrated.

1. Introduction

Monopiles support 81% of Offshore Wind Turbines (OWTs) in the North Sea due to their simplicity in design, fabrication, and installation (Wind Europe, 2021a). The UK is a global leader in offshore wind with a current capacity of 10.5 GW (Wind Europe, 2021b), aiming to generate 40 GW by 2030 (DECC, 2011). However, OWTs are increasing in size due to a growing demand in renewable energy, which has made the use of existing design methodologies uncertain (API, 2014; DNV, 2021). Larger pile diameters are required to ensure the superstructure remains within allowable deflection tolerances, which introduces new soil resistance mechanisms due to the semi-rigid behaviour of the pile (Lam, 2013; Byrne et al., 2017; Zhang and Andersen, 2019). The design of monopiles for OWTs is therefore becoming increasingly complex, and the need for simplified design methods is becoming more apparent.

The p-y method simplifies the soil–structure interaction to one horizontal dimension, utilising elastic beam elements to model the pile and nonlinear springs as soil elements to encapsulate soil behaviour. The springs are characterised by modelling the lateral soil pressure, p, as a nonlinear function of the lateral displacement of local pile section, y. This method is widely used in practice due to its simplicity and effectiveness in capturing the lateral response of piles (Reese et al., 1974; O'Neill and Murchison, 1983; Jeanjean et al., 2011; Lehane and Suryasentana, 2014). However, this methodology has been shown to be inadequate for modelling the lateral response of monopiles due to the additional resistance mechanisms that are not captured by the p-y method (Lam, 2013; Byrne et al., 2017; Zhang and Andersen, 2019; Van Impe and Wang, 2020). This type of model can successfully capture the lateral response of piles with high L/D ratios, where L is the embedded length of the pile and D is the pile diameter (Lehane and Suryasentana, 2014; Thieken et al., 2015; Amar Bouzid et al., 2013; Doherty and Gavin, 2011). The API approach is a common methodology (API, 2014), which was originally derived for oil and gas platforms supported by slender piles (high L/D) with low moment to horizontal load ratios (Cox et al., 1974; Reese et al., 1974; Murchinson and O'Neill, 1986). Monopiles are open-ended circular steel piles with L/D ratios typically ranging between 3 and 10 and are subject to large overturning moments from the superstructure, therefore extrapolating the API method is not appropriate (Kallehave et al., 2015; Byrne et al., 2017). Alternative methods for analysing soil–structure interaction are often required for low L/D substructures (Ali Jawaid and Madhav, 2013; Chen et al., 2022; Gerolymos and Gazetas, 2005).

* Corresponding author.
E-mail address: jacques.tott-buswell1@nottingham.ac.uk (J. Tott-Buswell).

https://doi.org/10.1016/j.oceaneng.2023.116642
Received 18 August 2023; Received in revised form 11 December 2023; Accepted 30 December 2023
Available online 6 January 2024

The PISA project aimed to improve the traditional *p-y* methodology by introducing additional spring types to encapsulate soil resistance mechanisms that are present for low L/D monopiles (Byrne et al., 2015). Known as diameter effects, relatively large pile diameters increase the presence of pile tip resistances under lateral loads, and the interface friction along the pile begins to resist rotation (Lam, 2013; Byrne et al., 2017; Zhang and Andersen, 2019; Van Impe and Wang, 2020). The PISA project calibrated soil reaction elements from pile push-over tests in sand and clay at sites with ground conditions similar to those found in offshore environments (Byrne et al., 2020b; McAdam et al., 2020; Zdravković et al., 2020a). These site tests are then used to inform three-dimensional finite element analyses such that one-dimensional reaction curves can be extracted to inform the beam–spring model (Zdravković et al., 2020b; Taborda et al., 2020). This process derived design tables for a range of L/D ratios and soil configurations that can be used for preliminary design, which can be improved using reaction curves extracted from bespoke three-dimensional finite element models when site-specific soil data is available (Byrne et al., 2019). This methodology has been shown to work well for a range of pile geometries in homogeneous and layered soils (Burd et al., 2020a,b; Byrne et al., 2020a). However, this can undermine the simplicity of beam–spring models, and offshore site conditions may not be comparable to those used in the PISA project.

OWTs are often installed in unique soil conditions for large wind farm arrays. It is therefore beneficial to take advantage of simplified one-dimensional methods that are mindful of the site variability to obtain initial estimates of pile dimensions. The Cone Penetration Test (CPT) is often the first ground investigation performed in the offshore environment, and can provide an early indication of the soil strength profile with depth. Many CPT-based *p-y* methodologies are available (Li et al., 2014; Novello, 1999; Dyson and Randolph, 2001; Suryasentana and Lehane, 2014, 2016), but are also limited to their calibration space. It is therefore beneficial to use CPT data to inform the soil reaction elements of a multi-spring model that can be used for preliminary design of monopiles, which can be further optimised when more rigorous site data is available.

The objective of this paper is to characterise spring elements for a multi-spring model using CPT data and to demonstrate the model's application to reported field test data. The soil elements to be characterised are (i) the distributed moment–rotation (m–θ) springs along the pile shaft, (ii) a moment spring at the pile base due to bearing stresses, and (iii) a lateral spring at the pile base to model shearing behaviour. The m-θ relationship is derived from existing CPT-based axial capacity methods (Lehane et al., 2020a,b). The pile tip elements are informed using CPT-based estimates of the post-installation bearing stress at the base of the pile (Burd et al., 2020b; Byrne et al., 2018). The *p-y* elements are defined from existing CPT-based formulations (Li et al., 2014). The model is intended for use in cohesionless soils and is not intended to provide an estimate of a monopile's ultimate lateral capacity. The derivation of the model components, and its application to reported field test data, are presented herein.

2. CPT-based multi-spring model

Fig. 1 illustrates the four anticipated resistances for a low L/D monopile when laterally loaded at the pile head by a force F at eccentricity h. The horizontal pile displacement y mobilises lateral soil pressures p and the local rotations θ induce a distributed interface shear that generates a moment m. The pile tip is subject to a moment M_b due to the bearing stresses $q_{b,res}$ and a horizontal shear force V_b due to lateral displacements at the tip. Assuming Winkler's theory, the reaction mechanisms can be treated as uncoupled and take the form of a *p-y* model with additional springs (Winkler, 1867), as shown in Fig. 1b.

Using the Direct Stiffness Method, the model shown in Fig. 1b can be discretised into elements and the displacement can be solved for (Tedesco, 1999). The monopile is modelled using four degree-of-freedom elastic beam elements, where each node is supported by lateral and rotational springs. Timoshenko beam theory is used to capture internal shear deflections within the pile section that are expected for low L/D monopiles (Gupta and Basu, 2018). Axial forces within the monopile are neglected. The nonlinear soil elements are described by updating the secant modulus of the reaction curves. The lateral soil pressure is captured using a *p-y* definition, and the distributed moment due to soil–pile interface friction is modelled as distributed m-θ spring elements. A lateral and rotational spring is added to the pile base to encapsulate tip resistances resulting from large diameter effects. The lateral base shear spring (V_b-y_b) models the lateral shearing due to the pile annulus and internal soil, and the base rotation spring (M_b-θ_b) represents the moment resistance incurred due to soil bearing stress $q_{b,res}$.

The CPT-based reaction curves for each new spring element are derived in the following sections.

2.1. Lateral p-y springs

p-y functions are commonly derived from site test data or finite element calibration procedures that are specific to a particular pile–soil configuration. This means that these functions are typically only suitable for use within a limited range of pile dimensions and soil profiles for which they were originally derived or calibrated (Jeanjean et al., 2011; O'Neill and Murchison, 1983; Lehane and Suryasentana, 2014; Reese et al., 1975; Murphy et al., 2018). When choosing a *p-y* function to inform the lateral resistance elements of a multi-spring model, it is necessary to isolate the lateral soil pressure p to prevent an overlap with other mechanical resistances that could be implicitly defined within the *p-y* relationship. Additionally, the *p-y* function must exhibit an appropriate consideration of the flexural rigidity of the pile, which can have a significant influence on the lateral resistance (Poulos and Hull, 1989; Ashford and Juirnarongrit, 2003; Fan and Long, 2005).

The power law *p-y* relationship proposed by Li et al. (2014) was derived using open-ended circular steel piles installed in siliceous sands, with L/D ratios ranging between 6.5 and 20. As slenderness ratios as low as 6.5 were considered, resistance mechanisms from the aforementioned diameter effects may be inherently included in its parametrisation space. Murphy et al. (2018) showed that, when $L/D = 6$, *p-y* springs can contribute to ~90% of resistance by evaluating the percentage contribution to resisting the applied overturning moment for each spring type. It is therefore assumed that the *p-y* relationship derived by Li et al. (2014) isolates the lateral soil pressure p when used in a multi-spring framework, as the L/D ratio of the most rigid pile in the calibration space is above $L/D = 6$ (Li et al., 2014). The intended L/D ratio for the *p-y* relationship is also low enough that appropriate pile flexibility may be assumed accounted for. To add, the function was derived for piles with the cross-sectional properties of a monopile. The *p-y* function is shown in Eq. (1).

$$p = 3.6D(\gamma' D)\left(\frac{q_c}{\gamma' D}\right)^{0.72}\left(\frac{y}{D}\right)^{0.66} \tag{1}$$

where γ' is the effective unit weight of sand.

It should be noted that Li's *p-y* function cannot be used to model the ultimate lateral capacity of piles due to the power law relationship. As such, the multi-spring model is limited to small to medium range deflections and cannot fulfil ULS design. However, it may still be used to estimate the initial response and deflection range of a monopile within typical operational deflections, as loading conditions that reach the designed ultimate capacity are seldom experienced during OWT operation.

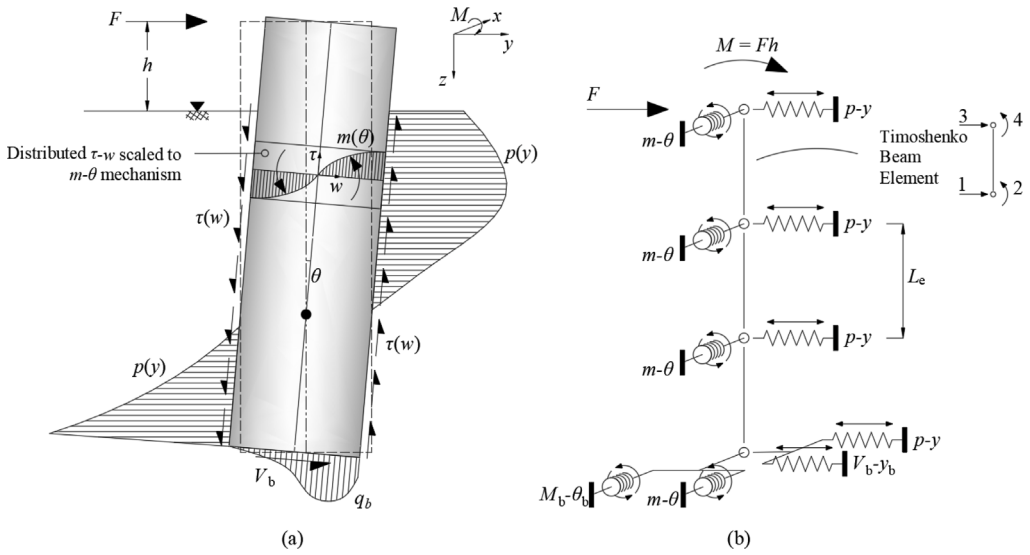

Fig. 1. (a) Resistances for monopiles under lateral loading and (b) schematic of discretised multi-spring model.

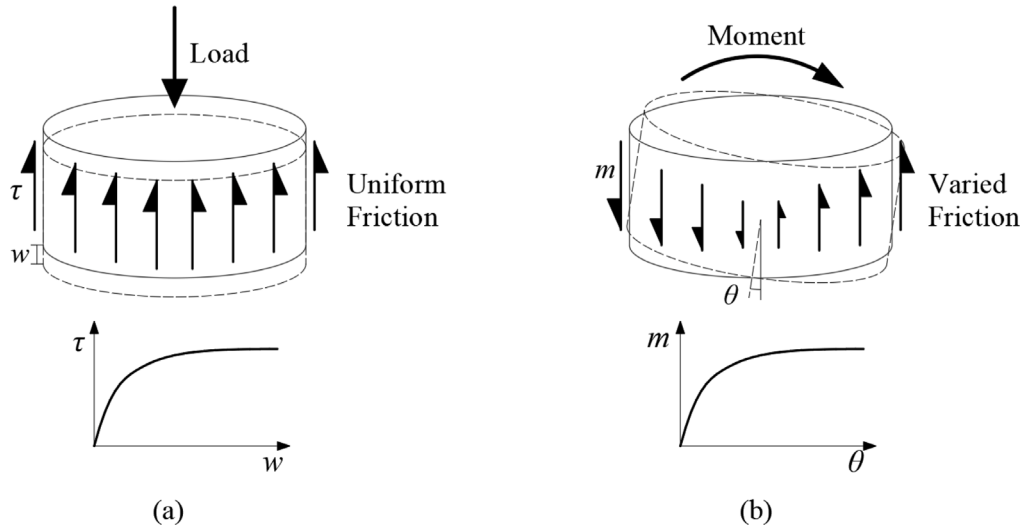

Fig. 2. (a) Axial model with uniform friction and (b) rotational model with varied friction.

2.2. Rotational m-θ springs

The distributed moment m due to the vertical soil–pile interface friction becomes more significant as the diameter of the monopile increases (Lam, 2013; Byrne et al., 2015). This is due to the pile radius acting as a lever arm as the pile rotates, which is not explicitly captured in traditional p-y models. The moment–rotation relationship of this spring element can be informed using vertical shear-displacement reaction curves (τ-w) mapped to a moment–rotation function (m-θ), as demonstrated in Fig. 2. The distributed τ-w curves are well-defined in CPT-based axial capacity design methodologies (Lehane et al., 2020a), therefore a CPT-based m-θ function can be derived.

The τ-w relationship is described in Eq. (2) as defined by Lehane et al. (2020a):

$$\tau = G_0\left(\frac{w}{2D}\right)\left[1-\frac{w}{2w_f}\right] \tag{2}$$

where w_f is the local ultimate displacement and is defined as $4D\tau_f/G_0$, G_0 is the initial shear modulus of the soil and τ_f is the local maximum vertical shaft shear resistance. G_0 and τ_f are the only parameters required for full definition of the τ-w relationship and can be estimated using appropriate CPT q_c correlations in the absence of appropriate site test data. For example, G_0 can be approximated with q_c using empirical scaling relationships such as those proposed by Baldi et al. (1989) as recommended in the IC-05 design method (Jardine et al., 2005).

It is expected that dilation and plugging effects are present for small-scale steel open-ended circular piles, which can have an effect on pile–soil interface shearing capacities (Lehane and Gavin, 2001; Gavin et al., 2013; Lehane et al., 2005). To enable meaningful comparisons with scaled monopile site tests, it is important that this behaviour is encapsulated in the multi-spring model. The CPT-based design methodology estimates the pile shaft friction at approximately 14 days after driving and is shown in Eq. (3) (Lehane et al., 2020a).

$$\tau_f = \left(\frac{f_t}{f_c}\right)\left(\sigma'_{rc}+\Delta\sigma'_{rd}\right)\tan\delta_f \tag{3a}$$

$$\sigma'_{rc} = \left(\frac{q_c}{44}\right)A_{re}^{0.3}\left[\max\left(1,\frac{H}{D}\right)\right]^{-0.4} \tag{3b}$$

$$\Delta\sigma'_{rd} = \left(\frac{q_c}{10}\right)\left(\frac{q_c}{\sigma'_v}\right)^{-0.33}\left(\frac{d_{\mathrm{CPT}}}{D}\right) \tag{3c}$$

where f_t/f_c is the loading configuration ratio, A_{re} is the effective area ratio, H is the distance from the pile tip to the soil horizon of

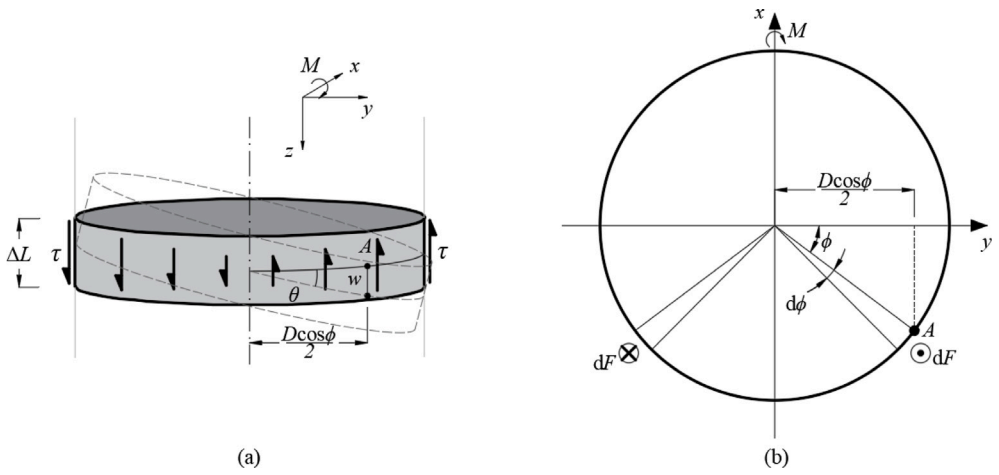

Fig. 3. (a) section side view under rotation (b) section plan view with varying shear force.
Source: Modified from Fu et al. (2020).

interest, σ'_v is the effective vertical stress ($\gamma' z$), d_{CPT} is the diameter of the standard CPT probe (35.7 mm), and δ_f is the interface friction angle (defined as 29° in Lehane et al., 2020a). f_t/f_c is taken as 0.8 for general applications, as suggested by O'Neill (2001). Eq. (3b) represents the radial effective stress induced by plugging, where $A_{re} = 1 - \mathrm{PLR}(D_i/D)^2$ and PLR is the Plug Length Ratio (defined as $\mathrm{PLR} = \tanh(0.3(D_i/d_{\mathrm{CPT}})^{0.5})$). $D_i = D - t$, where t is the wall thickness of the pile and D_i is the internal diameter.

σ'_{rc} encapsulates the effects due to soil plugging expected for an open-ended pile, and $\Delta\sigma_{rd}$ represents the increase in radial effective stress due to dilation. Both σ'_{rc} and $\Delta\sigma'_{rd}$ are inversely proportional to the pile diameter, therefore the function can be extrapolated to larger pile configurations where plugging effects are less pronounced and full coring behaviour can be expected (i.e. soil within the full depth of the pile post-installation) (Lehane et al., 2020b).

Fig. 3 illustrates how the friction forces vary around the pile circumference with respect to the polar angle ϕ. The relative local vertical deflection w can be described using Eq. (4).

$$w = \frac{\theta D}{2}\cos\phi \tag{4}$$

The distributed moment per unit of resistance is:

$$m = 2\int_{-\pi/2}^{\pi/2} \frac{D}{2}\cos\phi\, dF \tag{5}$$

It is important to note that the factor 2 assumes a symmetrical distribution of frictional forces about the pile, meaning the shear stiffness of the sand is assumed isotropic around the circumference of the pile. The local interface shear resistances on the active and passive sides of the pile will become progressively more asymmetric for increasing lateral displacements due to the changes in lateral soil pressures expected when loaded horizontally. Whilst symmetrical interface shearing is an unrepresentative approximation at large deflections, it is assumed that the change in the generated moments on both sides of the pile section are partially conserved when moments are taken about the axis of rotation of the pile. The resulting moment from the increasing interface shear on the passive side and decreasing interface shear on the active side is assumed to remain unchanged. Interface gaps and significant asymmetry in the soil stresses around the pile section are assumed negligible for the small to medium deflection range of interest, but may be significant for large deflections.

Substituting $dF = \tau dA$ (where $dA = 0.5Dd\phi$) into Eq. (5) gives m as a function of $\tau(w)$.

$$m = \frac{D^2}{2}\int_{-\pi/2}^{\pi/2} \tau(w)\cos\phi d\phi \tag{6}$$

Table 1
Key parameters of the m-θ function.

Parameter	Definition
Maximum moment, m_f	$a^2/4b = \frac{3}{32}\pi^2 D^2 \tau_f$
Failure rotation, θ_f	$a/2b = 3\pi\tau_f/G_0$
Initial rotation stiffness, k_θ	$a = \pi D^2 G_0/16$

Substituting Eq. (3) into (2) and subsequently Eq. (2) into (6), then solving the integral gives the total moment per unit length m as a parabolic function of θ:

$$m(\theta) = \begin{cases} a\theta - b\theta^2 & \theta < \theta_f \\ m_f & \theta \geq \theta_f \end{cases}$$
$$a = \frac{G_0 D^2 \pi}{16}, \quad b = \frac{G_0^2 D^2}{96\tau_f} \tag{7}$$

where m_f is the ultimate moment capacity per unit length and θ_f is the rotation at capacity. Full parametrisation of the m-θ function is shown in Table 1, including the initial stiffness k_θ.

2.3. Base moment M_b-θ_b spring

CPT-based correlations to estimate the moment resistance at the pile tip due to overturning are not well-defined in literature, therefore cautious estimates are made herein. A residual bearing stress $q_{b,res}$ at the pile base exists post-installation (Byrne et al., 2018) and can resist tip rotation. This can have a significant influence on the lateral resistance of low L/D monopiles (Burd et al., 2017). Byrne et al. (2018) investigated the impact of $q_{b,res}$ on the driveability of piles by estimating the residual stress as a function of the cone tip resistance local to the base ($q_{c,r}$). Defined as $q_{b,res} = \alpha q_{c,r}$, the parameter α was varied to achieve a best fit to data from driven pile site tests. It was found that residual bearing stresses exist even for large diameter piles installed with no plugging effects (Byrne et al., 2018).

$q_{c,r}$ should be chosen in a way that accounts for the variation in the local q_c values near the pile tip. In this study, $q_{c,r}$ is taken as the average q_c over a range above and below the pile tip. This range is set as a function of L/D, as monopiles with smaller L/D values tend to be more sensitive to variations in soil strength near the tip. This way the range is proportional to the slenderness ratio and will appropriately decrease for low L/D monopiles. It is important to note that the range will become disproportionately large for piles with a high L/D, but the influence of the tip resistance will become insignificant in this case. The range is taken as $0.25L/D$ above and below the pile tip, which was

deemed appropriate for the piles and CPT profiles used in this study. However, this value is at the discretion of the user.

A bilinear relationship is used to simplify the quantification of the anticipated nonlinear relationship. For simplicity, the restoring moment at the tip is assumed to act over a semi-circular area on the pile base. The maximum moment at the base is described in Eq. (8).

$$M_{b,f} = q_{b,res}\frac{\pi D^2}{8}d \tag{8}$$

where d is the lever arm and is taken as $2D/3\pi$, which defines the distance from the centroid of the loaded semicircular area to the centre of the pile cross section.

The PISA one-dimensional model has underlying similarities to the multi-spring model presented herein (Burd et al., 2020a,b; Byrne et al., 2020a). Each spring is characterised using a dimensionless conic function that provides a convenient means to calibrate soil reactions to relevant displacement/rotation variables (Burd et al., 2020b). The function's ultimate soil reaction, initial stiffness, and displacement/rotations are derived based on three-dimensional finite element analysis calibration procedures of piles in dense sand (Burd et al., 2020b), informed from soil sample tests extracted from the Dunkirk site test (Zdravković et al., 2020a). All normalisation parameters for the conic function were determined based on a calibration space of $2 \leq L/D \leq 6$ and $45\% \leq D_r \leq 90\%$. From calibration procedures described in Burd et al. (2020b), the failure rotation for a moment–rotation spring at the pile tip is given as:

$$\theta_{b,f} = \frac{\bar{\theta}_b \sigma'_b}{G_0} \tag{9}$$

where σ'_b is the vertical effective stress at the pile base and $\bar{\theta}_b$ is the calibrated ultimate rotation dimensionless parameter, taken as 44.98 (Burd et al., 2020b). Note that $\bar{\theta}_b$ is determined for piles with slenderness ratios between 2 and 6, therefore its application to piles with $L/D > 6$ is uncertain. However, it is expected that the moment induced at the pile tip will be increasingly insignificant for smaller diameters (higher L/D ratios) due to the D^3 term implicit in Eq. (8).

2.4. Base shear V_b-y_b spring

For large diameter monopiles, the soil within the annulus of the cross-section will undergo horizontal shearing when the pile head is laterally loaded. It is assumed that the residual bearing stress $q_{b,res}$ acts as the confining stress, such that the horizontal shear at the base ($\tau_{b,f}$) can take a Mohr–Coulomb assumption. It is expected that the soil within the annulus of the pile tip will be both pre-stressed and densified by the pile installation mode. As CPT-based correlations that estimate the friction angle within the pile at the tip are limited, a 35° angle is assumed for dense soil post-installation (Byrne et al., 2018). $\tau_{b,f}$ can therefore be approximated as $q_{b,res}\tan 35°$. The M_b-θ_b and V_b-y_b spring at the pile tip are both a function of the bearing stress post-installation.

The V_b-y_b load–displacement function assumes a bilinear relationship, where the capacity V_b is defined as the maximum shear force at the pile tip. Zhang and Andersen (2019) suggested that the scoop-like shearing mechanism expected at the tip of a rotating pile can be simplified to a horizontal shear across the pile section for large pile diameters. The shearing surface of the pile tip scoop and the pile tip area become increasingly similar as the diameter increases, therefore the shear force $\tau_{b,f}$ can be assumed to act over the area of the cross-section (Zhang and Andersen, 2019). The expected maximum shear force is therefore:

$$V_{b,f} = \frac{\pi D^2}{4} q_{b,res}\tan 35° \tag{10}$$

The failure displacement $y_{b,f}$ for the bilinear lateral base spring is informed based on the PISA methodology (Burd et al., 2020b) and is as follows:

$$y_{b,f} = \frac{2\bar{y}_{b,f} D\sigma'_b}{G_0} \tag{11}$$

$$\bar{y}_{b,f} = \bar{y}_{b,f1} + \bar{y}_{b,f2}\left(\frac{L}{D}\right) \tag{12}$$

where $\bar{y}_{b,f1} = 0.52 + 2.88D_r$ and $\bar{y}_{b,f2} = 0.17 - 0.70D_r$ and D_r is the relative density ($D_r = 0.75$ as recommended by Burd et al., 2020b).

Eqs. (11) and (12) are calibrated based on three-dimensional finite element analysis procedures and are used to define the normalised conic spring function that models local horizontal soil reactions at the pile tip. $\bar{y}_{b,f}$ is intended for $2 \leq L/D \leq 6$ and $45\% \leq D_r \leq 90\%$ (Burd et al., 2020b).

According to Eq. (12) it is possible for the initial stiffness of the bilinear base shear spring (i.e. $V_{b,f}/y_{b,f}$) to be negative or have an extremely large value for monopiles with large slenderness ratios. An arbitrary upper and lower limit of $L/D = 6$ and $L/D = 2$ are applied to Eq. (12) to remain within the calibration space and to prevent inadmissible stiffness values. Due to the second order power law relationship with respect to D in Eq. (10), small diameters (high L/D ratios) will reduce the expected shear force and consequently minimise the significance of these limits, but will not affect monopile geometries where base shearing is expected.

2.5. Calculation procedure

The pile deflections are computed using the Direct Stiffness Method (Tedesco, 1999), where $\{x\} = [K]^{-1}\{F\}$. The secant stiffness matrix $[K]$ is assembled from the individual secant stiffnesses of the spring elements and the elastic Timoshenko beam elements representing the pile. The nodal displacements $\{x\}$ are solved for using an iterative procedure where $[K]$ is updated with the secant stiffness of the spring elements until convergence is achieved. $\{F\}$ contains the force applied at the pile head, including the anticipated applied moment M at the ground line due to eccentricity h ($M = Fh$). The length of each beam element is set to $\Delta L = 0.05$ m. The elastic modulus, shear modulus, density and Poisson ratio are taken as 200 GPa, 80.77 GPa, 7850 kg m^{-3} and 0.3, respectively.

The CPT q_c profile is averaged at depth increments of 0.05 m, which is the same as the length of the beam element. The average q_c value is then used to inform the respective p-y and m-θ spring. $q_{b,res}$ is estimated as a percentage (α) of the average q_c value $0.25L/D$ above and below the pile tip. $\Delta L = 0.05$ m is a sufficiently small length to capture the spatial variability of the CPT profiles used in this study, and reducing the value has shown a negligible influence on results. The numerical model is developed in MATLAB, and the pile tests described in the following Sections are replicated using the multi-spring model and their respective CPT profile. The deflections at the ground line node are recorded for each applied load step and the results are compared to the reported field data.

The influence of the residual bearing stress $q_{b,res}$ on both the moment and shearing spring mechanisms at the pile tip remains uncertain and warrants further investigation. The subsequent analyses will evaluate the performance of the multi-spring model by comparing it to site tests conducted on laterally loaded piles. The parameter α is varied to identify an appropriate value for $q_{b,res}$ that aligns with the performance of site investigations. A maximum value of 0.1 is used, as recommended by Byrne et al. (2018).

3. Analysis and results

A wide range of monotonic push-over tests were performed at a site in Blessington, Ireland, investigating the influence of slenderness ratio for open-ended circular steel piles. Notable uniformity is demonstrated across the site (Doherty et al., 2012), therefore the average CPT profile is used to inform the multi-spring model. Site tests performed in Dunkirk, France, also investigated the performance of laterally loaded scaled monopiles, including local CPT q_c profiles for each pile's location (Zdravković et al., 2020a), enabling an improved investigation on the spatial variation sensitivity in CPT-based p-y models. Both site tests

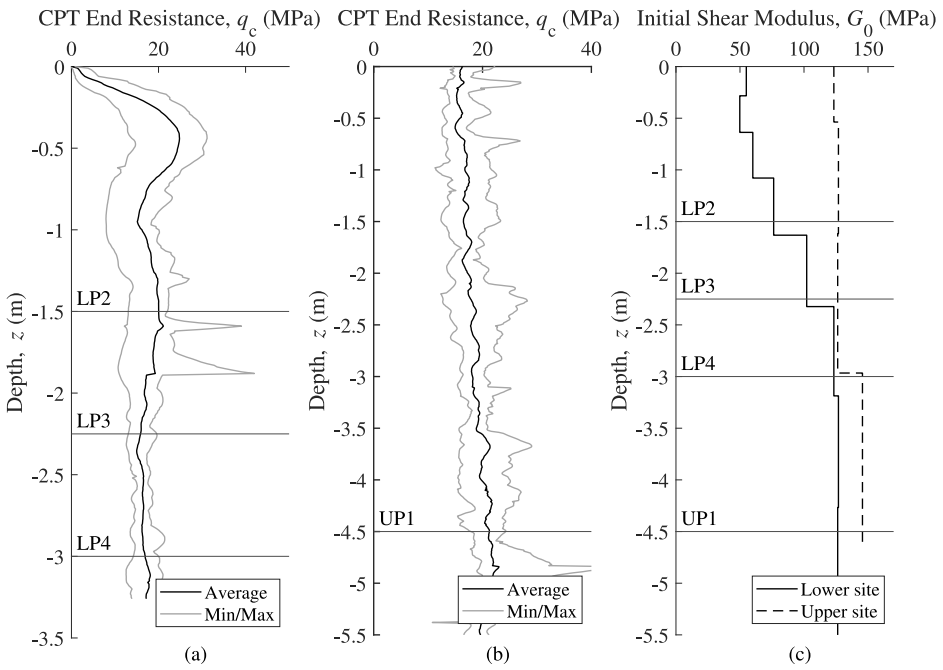

Fig. 4. (a) minimum, maximum and average q_c profiles for Blessington Lower quarry (b) minimum, maximum and average q_c profiles for Blessington Upper quarry (c) G_0 profile used for Blessington Upper and Lower quarry.

were performed in dry sand, therefore the influence of groundwater was not considered.

The SLS design philosophy for OWTs requires that the ground line rotations remain within 0.25° (DNV, 2021). However, only the ground line displacement was measured at the site tests used in this study. For this reason, it is assumed that 0.25° rotation is equivalent to $0.01D$ displacement at the ground line. This can be justified by assuming the rotation point of a laterally loaded rigid pile is located at $2/3L$ below the ground line (Arany et al., 2017; Chortis et al., 2020). Reported site tests in this investigation were incrementally loaded to capacity, therefore creep is evident in the ground lines response. However, the creep effects are expected to be minimal within the SLS deflection range.

3.1. Blessington tests

Lateral load tests were performed in two regions of the Blessington site, Dublin, and are described herein. Blessington Lower quarry (BL) comprised three monopile configurations with L/D = 3, 4.5, and 6; and one pile from Blessington Upper quarry (BU) with L/D = 13. Full details on pile dimensions are given in Table 2. Fig. 4 demonstrates the notable uniformity for the CPT investigations for each quarry. Due to the lack of pile-specific CPT data, the average q_c profile is used to inform the multi-spring model. The water table is reported to be 13 m below ground level for BU and >10 m below ground level for BL. The site contains dense, fine sand with relative density close to 100% and bulk unit weight of 19.8 kN m^{-3}. All piles were installed via driving. Detailed descriptions of the ground conditions at the Blessington site have been reported by Gavin and Lehane (2007), Tolooiyan and Gavin (2011) and Doherty et al. (2012). Minimum, maximum, and average CPT profiles, including the G_0 profile, are plotted in Fig. 4 for both BL and BU sites.

The piles described in Table 2 are modelled using the multi-spring model and the springs are informed using the average CPT and G_0 profile shown in Fig. 4. Three different permutations of the multi-spring model are simulated to demonstrate the individual spring-type contributions to lateral resistance. These permutations include the traditional p-y-only method, p-y + m-θ, and the full multi-spring model, which incorporates both rotational and lateral pile tip spring elements. The results are shown in Fig. 5. Two configurations of the multi-spring model are plotted; one with $q_{b,res} = 0.1q_{c,r}$ and the other corresponding to the $q_{b,res}$ value that provides the best fit to pile head deflections.

Table 2
Monopile geometries at Blessington site (Murphy et al., 2018).

Pile Name	Embedment L (mm)	Diameter. D (mm)	Slenderness ratio L/D	Thickness t (mm)	Eccentricity h (mm)
LP2	1500	510	3.0	10	1000
LP3	2250	510	4.5	10	1000
LP4	3000	510	6.0	10	1000
UP1	4500	340	13.0	14	400

The multi-spring model compares well with the site tests for all piles at deflections below $0.01D$ when $q_{b,res} = 0.1q_{c,r}$, which can be improved for larger deflections if an appropriate $q_{b,res}$ value is identified. Notably, the response of different spring model permutations demonstrate that the influence of each spring type diminishes as the slenderness ratio increases. For example, the difference between the deflection estimated in the p-y +m-θ model and the p-y-only model is greater for piles with low L/D ratios, such as piles LP2 and LP3 in Fig. 5a and b, respectively. This is indicative of the contribution of the distributed m-θ springs, and reduces for the more flexible piles such as LP4 and UP1, as shown in Fig. 5c and d, respectively. Pile UP1 indicates that, when L/D is high, the additional spring mechanisms become negligible and the multi-spring model collapses to the traditional p-y method. This is suggested in Fig. 5d, as the difference between the p-y and multi-spring model is minor, and demonstrates that the diameter effects present in low L/D monopiles are captured effectively in the proposed model. It is worth noting that the apparent underestimation of ground line deflections in UP1 could potentially be attributed to the use of a site-averaged CPT profile.

The p-y function proposed by Li et al. (2014) is a power law relationship and is calibrated for piles with $L/D \geq 6.5$, therefore it is not suitable for the response prediction of low L/D piles loaded to failure. This is evident in Fig. 5a and b, as the p-y -only model does not capture the yielding behaviour of piles LP2 and LP3. A more appropriate p-y function should be applied if ULS analysis is required.

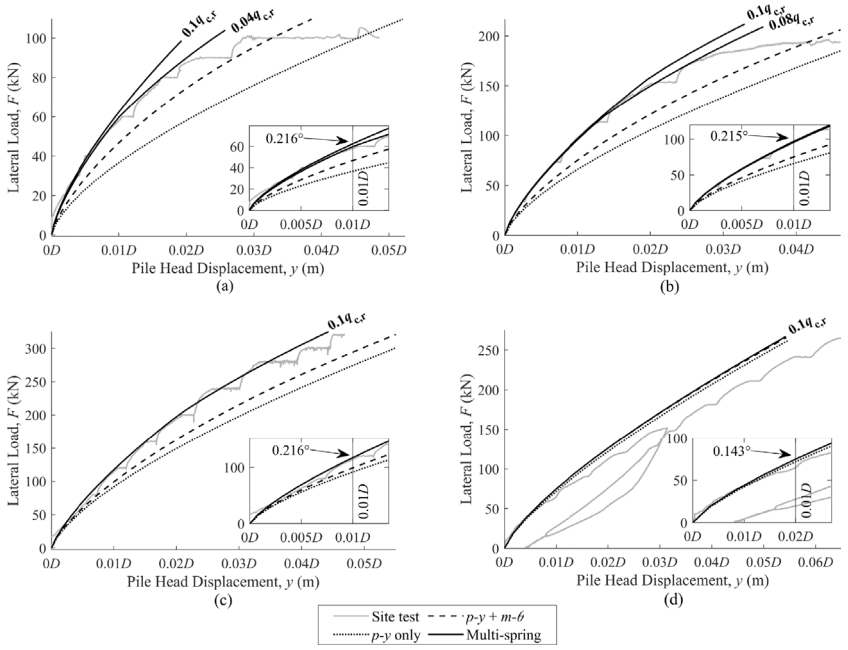

Fig. 5. Model performance compared to Blessington pile tests (a) LP2, $L/D = 3.0$ (b) LP3, $L/D = 4.5$ (c) LP4, $L/D = 6.0$ (d) UP1, $L/D = 13.0$.

The issue is further exaggerated by the significant creep experienced at large ground line deflections, which is not considered in the proposed model.

When $q_{b,res} = 0.1q_{c,r}$, the multi-spring model offers a satisfactory match to all the pile tests conducted at Blessington for small deflections below $0.01D$, and are within the ground line rotation limit of 0.25°. However, the ground line deflection at higher loads is underestimated for low L/D piles, giving a conservative estimate. Notably, LP2, LP3, and LP4 require different $q_{b,res}$ values ($0.04q_{c,r}$, $0.08q_{c,r}$, and $0.1q_{c,r}$, respectively) to improve large head deflection estimates. This observation suggests that $q_{b,res}$ increases with the L/D ratio. However, determining precise correlations for parameters localised near the pile tip remains challenging due to the many factors that influence ground line deflections. Furthermore, the utilisation of an average CPT profile across the site limits the ability to directly investigate such correlations. It is also important to address that changing the p-y function will influence the perceived value of $q_{b,res}$ required for large deflection estimates, suggesting different α values would arise for different p-y functions.

Accurate measurements of residual base stresses on open-ended piles in sand are scarce. For instance, Gavin and O'Kelly (2007) found that the residual base stress was linked to the Incremental Filling Ratio (IFR) during driving, pile diameter, and end resistance values. Similarly, Paik et al. (2003) reported a residual base stress of approximately 1.7 MPa, or around 6% of the q_c value at the pile tip, for a pile with a diameter of 0.356 m and an IFR of 75% at the end of driving. Another study by Gavin and Igoe (2021) measured very low residual stresses during the initial driving stages of a 0.34 m diameter pile when the IFR was high. Towards the end of installation, with an IFR value of 40%, a residual base stress of 4 MPa was mobilised, approximately 20% of the q_c value at the pile tip. Considering the substantial diameter of offshore monopiles, significant plugging during installation is unlikely. Therefore, it is recommended that residual stresses are conservatively estimated, and designers should exercise caution.

3.2. Dunkirk tests

The PISA project conducted a series of lateral push-over tests in Dunkirk (France) and Cowden (UK) to assess piles loaded in soil deposits similar to those encountered in offshore environments (Burd et al., 2020b; McAdam et al., 2020; Zdravković et al., 2020a). Twelve open-ended circular steel piles with various L/D ratios ranging from 3 to 8 were investigated. For this study, seven pile tests were selected from the literature, and are detailed in Table 3.

Table 3
Monopile geometries at Dunkirk site (McAdam et al., 2020).

Pile Name	Embedment L (mm)	Diameter. D (mm)	Slenderness ratio L/D	Thickness t (mm)	Eccentricity h (mm)
DM3	6000	762	8.00	25	10 000
DM4	4000	762	5.25	14	10 000
DM7	2250	762	3.00	10	10 000
DS1	1450	273	5.25	7	5000
DS2	1450	273	5.25	7	5000
DL1	10 600	2000	5.25	38	9900
DL2	10 600	2000	5.25	38	9900

CPT investigations were conducted at each pile location and the profiles are shown in Fig. 6a. This enables a meaningful evaluation of the influence of spatial variability on the CPT-based multi-spring model. The water table was found to be at a depth of $z = 5.4$ m below ground level, with soil bulk unit weights of $\gamma = 17.1$ kN m^{-3} and 19.9 kN m^{-3} above and below the water table, respectively. Fig. 6b presents the G_0 profile, which was computed using a combination of triaxial tests and seismic CPTs. Additional site-specific information is available in Zdravković et al. (2020a).

The majority of pile tests were subject to incremental loading at an average rate of 0.91 mm/min. DS2 was loaded continuously at a rate of 325 mm/min to investigate the influence of load rate on pile response. Notably, DS1 and DS2 share the same pile geometry but differ in terms of the load application rate. DS2 is included in this investigation to assess the influence of CPT profiles for identical pile geometries. It is worth noting that the proposed multi-spring model remains independent of load rate, which adds interest to evaluating the extent to which CPT variations influence pile response. Finally, DL1 and DL2 are included in this analysis for the same reason. Piles DL1 and DL2 were loaded against each other, and deflection measurements were recorded at the same time. Fig. 7 shows the results.

Similar to the Blessington site tests, the multi-spring model compares well with the site tests for all piles at deflections below $0.01D$

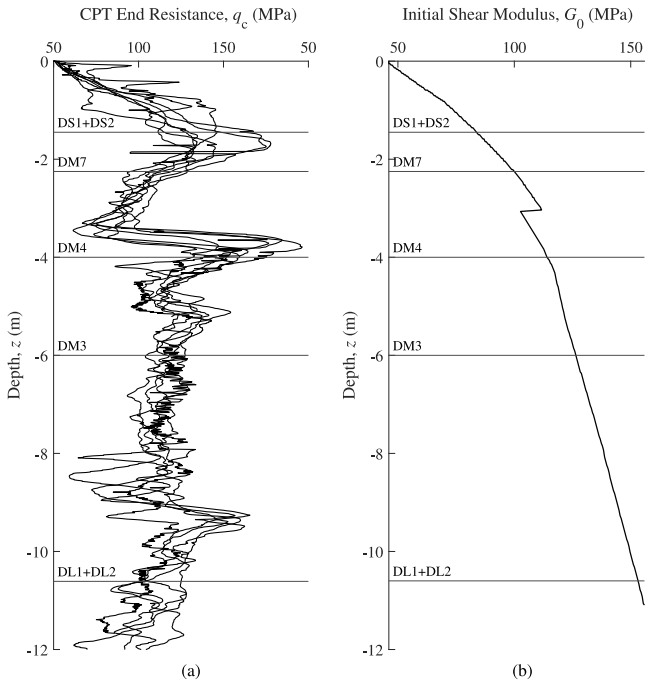

Fig. 6. (a) q_c profiles and (b) G_0 profile for the Dunkirk site (Zdravković et al., 2020a).

when $q_{b,res} = 0.1q_{c,r}$. Fig. 7a and c suggest that piles DM7 and DS1 exhibit an improvement in estimating the response when additional spring components are included, and an appropriate $q_{b,res}$ value can be identified to improve medium to large strain deflections. Furthermore, these results demonstrate that low L/D piles benefit from low α values to improve estimates for large displacements, which is a similar trend to that observed in the Blessington site tests.

Fig. 7d and b show that all spring model permutations exhibit a superficially stiff response in comparison to the DM3 and DM4 site tests. Notably, the estimated ground line deflections do not improve when more spring elements are added. This suggests that the issue is not entirely related to the additional resistance mechanisms proposed in this study. Fig. 6a shows that piles DM3 and DM4 are subject to excessive variability in q_c along the depth of the pile. In contrast, other pile tests, including those from the Blessington site, have either partially uniform or linearly increasing CPT end resistance profiles. To add, DS1 and DM4 both have a slenderness ratio of 5.25. Aside from differences in scale between the two pile geometries, a key distinction between DS1 and DM4 lies in the variability of the q_c inputs, as shown in Fig. 6. This suggests that high variations in q_c can lead to artificially large stiffness in p-y-only models. The q_c discretisation method proposed may not adequately account for the horizontal shear load transfer between sand layers and localised failures at regions carrying locally elevated loads. This may be a limitation with CPT-based p-y models in general.

According to Fig. 7c, pile DS1 exhibits a significant contribution from the base spring components, as the difference between the deflections estimated from the multi-spring model ($q_{b,res} = 0.1q_{c,r}$) and the p-y +m-θ model is large. This may be a consequence of the linearly-increasing CPT profile evident in Fig. 6, which ultimately causes a high stiffness in the base springs relative to the other reaction elements.

The initial deflections are captured reasonably well regardless of the issues associated with high CPT variation and uncertainty associated around $q_{b,res}$. It can be concluded that the CPT-based multi-spring model works best for relatively uniform CPT end resistance profiles, as a high degree of spatial variability leads to superficially stiff springs.

3.3. Sensitivity to CPT profiles

DS1, DS2, DL1 and DL2 offer an opportunity to investigate the influence of CPT profile variations for identical pile geometries. For the following analysis, $q_{b,res} = 0.1q_{c,r}$ is taken for piles DL1 and DL2, and $q_{b,res} = 0.06q_{c,r}$ for piles DS1 and DS2, as suggested by Fig. 7c.

As DS1 and DS2 were loaded at different rates (0.91 mm/min and 325 mm/min, respectively), it was originally concluded that the apparent stiffness difference between DS1 and DS2 can be attributed to the isotach behaviour of soil (McAdam et al., 2020). However, in Fig. 8a, it is observed that the multi-spring model provides reasonable ground line deflection estimates for both DS1 and DS2. More importantly, the model captures the apparent increase in stiffness in DS2. This suggests that the difference in load rate alone does not account for the observed change in resistance between piles DS1 and DS2. The multi-spring model is independent of load rate, which implies that these differences may be attributed, at least in part, to the local variations present in each CPT profile.

Fig. 8b shows that the multi-spring model underestimates ground line deflections beyond $0.01D$ and does not adequately capture the response of both DL1 and DL2. Again, this is likely due to substantial depth variations in the CPT profiles demonstrated in Fig. 6, leading to a superficially high stiffness in the model. Regardless, the model performs reasonably well for displacements below $0.01D$, and captures the relative difference between the deflections of DL1 and DL2.

4. Conclusions

A one-dimensional CPT-based multi-spring Winkler model has been developed, where each soil element is informed using discretised q_c data. The traditional p-y method is modified by incorporating additional spring mechanisms that encapsulate the expected resistances induced by diameter effects in low L/D monopiles. CPT-based axial capacity methods are repurposed to approximate distributed moment-resistances along the monopile, which arise from the rotation of large-diameter sections. Pile tip resistances are estimated by decoupling the expected base moment and horizontal shear mechanisms and utilising a rotational and lateral bilinear spring positioned at the pile base. The capacity of each base spring is informed by averaging q_c values $0.25L/D$ above and below the pile tip to estimate the post-installation residual bearing stress, $q_{b,res}$. The following conclusions are made:

1. The proposed model captures initial ground line deflections below $0.01D$ well when $q_{b,res} = 0.1q_{c,r}$, which is in agreement with SLS design criteria. It is not suitable for analysing large strains or predicting ultimate failure loads.
2. Determining an appropriate value for residual bearing stress ($q_{b,res}$) is challenging, and a conservative estimate of $q_{b,res} = 0.1q_{c,r}$ is recommended.
3. The m-θ, V_b-y_b, and M_b-θ_b springs successfully encapsulate diameter effects for low L/D monopiles, and become negligible as the slenderness ratio increases.
4. The model works well for CPT profiles that are uniform or linearly increasing with depth, such as those measured in the Blessington site.
5. Minor variations in CPT profiles are captured by the model. However, a high degree of spatial variability leads to a superficially stiff response.
6. A more appropriate p-y function is required to capture the ultimate capacity of the pile.

It is difficult to establish $q_{b,res}$ for lateral pile analysis using ground line deflection estimates, as there are many overlapping factors that influence the ground line response of a laterally loaded pile. Additionally, the underlying assumptions of uncoupled springs may not be suitable for CPT profiles of high variability, as the horizontal shearing between

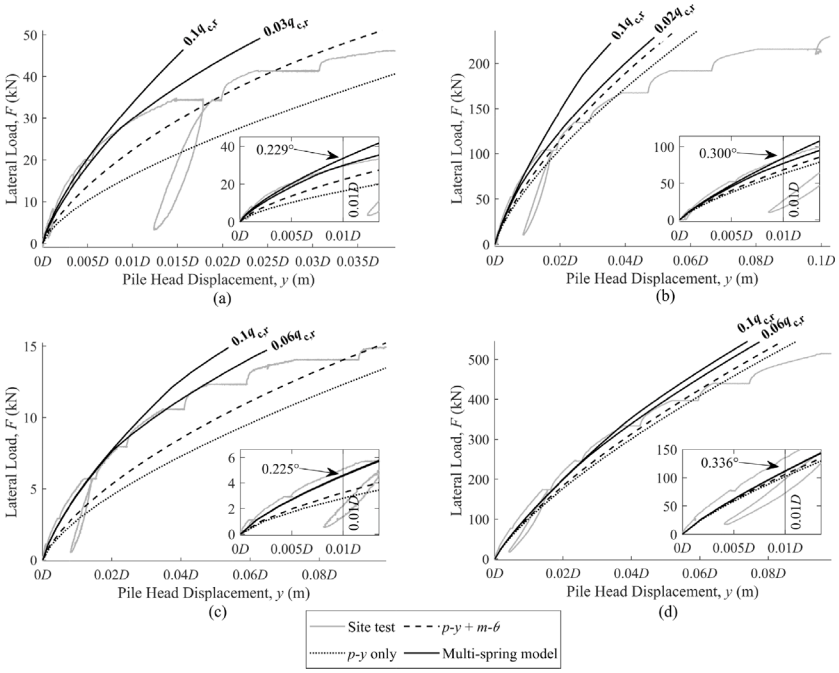

Fig. 7. Model performance compared to Dunkirk pile tests (a) DM7, $L/D = 3.0$ (b) DM4, $L/D = 5.25$ (c) DS1, $L/D = 5.25$ (d) DM3, $L/D = 8.0$.

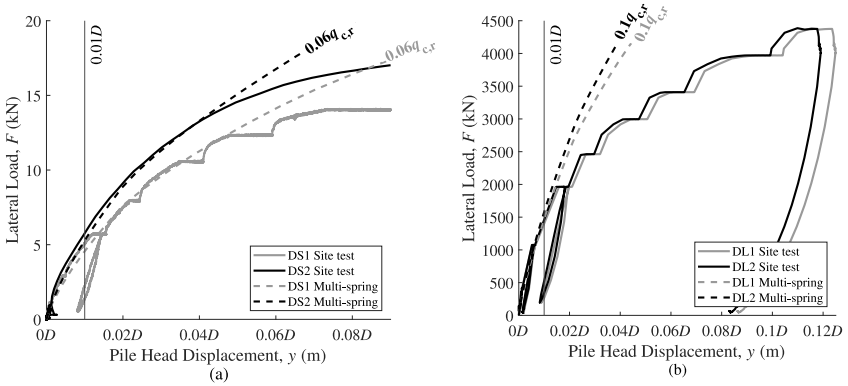

Fig. 8. Multi-spring model performance against pile tests DS1 and DS2 (b) Multi-spring model performance against pile tests DL1 and DL2.

laterally loaded soil layers is not captured. This may be significant for neighbouring soil horizons with large differences in q_c. It is postulated that utilising site-average q_c profiles may be more appropriate than CPT profiles local to the pile, as the model performed better in general for Blessington tests compared to Dunkirk tests. Averaging may reduce the degree of fluctuation within the input data and improve the model's performance. However, more data from site tests is required to support this claim.

The proposed model is a step towards a more comprehensive CPT-based model for laterally loaded monopiles. However, further work is required to improve the model's ability to capture the ultimate capacity of the pile. This may be achieved by defining a more suitable *p-y* relationship. This was not within the scope of this investigation, however the multi-spring model offers a modular framework to replace the current definition, should a more appropriate CPT-based *p-y* definition be proposed. To add, some underlying assumptions will require further modification. For example, the *m-θ* soil element assumes no gapping at large pile deflections and vertical interface shear stresses remain symmetrical about the pile section's central axis. This can be improved by coupling the *m-θ* element with the *p-y* element, as the confining stress imposed by the lateral soil pressure *p* will have an influence on the amount of vertical shear experienced. This is a topic of interest for future research.

CRediT authorship contribution statement

Jacques Tott-Buswell: Conceptualization, Formal analysis, Investigation, Methodology, Project administration, Software, Validation, Visualization, Writing – original draft, Writing – review & editing. **Luke J. Prendergast:** Funding acquisition, Supervision, Writing – review & editing. **Kenneth Gavin:** Data curation, Resources, Supervision, Writing – review & editing.

Declaration of competing interest

The authors declare that they have no known competing financial interests or personal relationships that could have appeared to influence the work reported in this paper.

Data availability

The authors do not have permission to share data.

Acknowledgements

The first author wishes to acknowledge funding for his PhD under EP/R513283/1 EPSRC Standard Research Studentship (DTP) at the Faculty of Engineering, University of Nottingham. The second author wishes to acknowledge the Faculty of Engineering at University of Nottingham for travel funding to facilitate this collaboration with Delft University.

References

Ali Jawaid, S.M., Madhav, M.R., 2013. Analysis of axially loaded short rigid composite caisson foundation based on continuum approach. Int. J. Geomech. 13 (5), 636–644. http://dx.doi.org/10.1061/(ASCE)GM.1943-5622.0000185.

Amar Bouzid, D.J., Bhattacharya, S., Dash, S.R., 2013. Winkler springs (p-y curves) for pile design from stress-strain of soils: FE assessment of scaling coefficients using the mobilized strength design concept. Geomech. Eng. 5 (5), 379–399. http://dx.doi.org/10.12989/gae.2013.5.5.379.

API, 2014. RP 2GEO: Geotechnical and Foundation Design Considerations. API, Washington, DC, USA.

Arany, L., Bhattacharya, S., Macdonald, J., Hogan, S., 2017. Design of monopiles for offshore wind turbines in 10 steps. Soil Dyn. Earthq. Eng. 92, 126–152. http://dx.doi.org/10.1016/j.soildyn.2016.09.024.

Ashford, S.A., Juirnarongrit, T., 2003. Evaluation of pile diameter effect on initial modulus of subgrade reaction. J. Geotech. Geoenviron. Eng. 129 (3), 234–242. http://dx.doi.org/10.1061/(asce)1090-0241(2003)129:3(234).

Baldi, G., Bellotti, R., Ghionna, V., Jamiolkowski, M., Lo Presti, D., 1989. Modulus of sands from CPTs and DMTs. In: Proc. 12th International Conference on Soil Mechanics and Foundation Engineering, Rio de Janeiro, 1989. Vol. 1. pp. 165–170.

Burd, H.J., Abadie, C.N., Byrne, B.W., Houlsby, G.T., Martin, C.M., McAdam, R.A., Jardine, R.J., Pedro, A.M.G., Potts, D.M., Taborda, D.M.G., Zdravković, L., Andrade, M.P., 2020a. Application of the PISA design model to monopiles embedded in layered soils. Géotechnique 70 (11), 1067–1082. http://dx.doi.org/10.1680/jgeot.20.PISA.009.

Burd, H.J., Byrne, B.W., McAdam, R., Houlsby, G.T., Martin, C.M., Beuckelaers, W.J.A.P., Zdravković, L., Taborda, D.M.G., Potts, D.M., Jardine, R.J., Gavin, K.G., Doherty, J.P., Igoe, D.J.P., Gretlund, J.S., Pacheco, M.A., Wood, A., 2017. Design aspects for monopile foundations.

Burd, H.J., Taborda, D.M.G., Zdravković, L., Abadie, C.N., Byrne, B.W., Houlsby, G.T., Gavin, K.G., Igoe, D.J.P., Jardine, R.J., Martin, C.M., McAdam, R.A., Pedro, A.M.G., Potts, D.M., 2020b. PISA design model for monopiles for offshore wind turbines: Application to a marine sand. Géotechnique 70 (11), 1048–1066. http://dx.doi.org/10.1680/jgeot.18.P.277.

Byrne, B.W., Burd, H.J., Zdravkovic, L., Abadie, C.N., Houlsby, G.T., Jardine, R.J., Martin, C.M., McAdam, R.A., Pacheco Andrade, M., Pedro, A.M., Potts, D.M., Taborda, D.M., 2019. PISA design methods for offshore wind turbine monopiles. In: Day 1 Mon, May 06, 2019. OTC, Houston, Texas, D011S005R002. http://dx.doi.org/10.4043/29373-MS.

Byrne, T., Gavin, K., Prendergast, L.J., Cachim, P., Doherty, P., Chenicheri Pulukul, S., 2018. Performance of CPT-based methods to assess monopile driveability in north sea sands. Ocean Eng. 166, 76–91. http://dx.doi.org/10.1016/j.oceaneng.2018.08.010.

Byrne, B.W., Houlsby, G.T., Burd, H.J., Gavin, K., Igoe, D.J.P., Jardine, R.J., Martin, C.M., McAdam, R.A., Potts, D.M., Taborda, D.M.G., Zdravković, L., 2020a. PISA design model for monopiles for offshore wind turbines: Application to a stiff glacial clay till. Geotechnique 70 (11), 1030–1047. http://dx.doi.org/10.1680/jgeot.18.P.255.

Byrne, B.W., McAdam, R.A., Burd, H.J., Beuckelaers, W.J.A.P., Gavin, K.G., Houlsby, G.T., Igoe, D.J.P., Jardine, R.J., Martin, C.M., Muir Wood, A., Potts, D.M., Skov Gretlund, J., Taborda, D.M.G., Zdravković, L., 2020b. Monotonic laterally loaded pile testing in a stiff glacial clay till at cowden. Géotechnique 70 (11), 970–985. http://dx.doi.org/10.1680/jgeot.18.PISA.003.

Byrne, B.W., McAdam, R., Burd, H.J., Houlsby, G.T., Martin, C.M., Beuckelaers, W.J.A.P., Zdravkovic, L., Taborda, D.M.G., Potts, D.M., Jardine, R.J., Ushev, E., Liu, T., Abadias, D., Gavin, K., Igoe, D., Doherty, P., Gretlund, J., Andrade, M.P., Wood, A.M., Schroeder, F.C., Turner, S., Plummer, M.A.L., 2017. PISA: new design methods for offshore wind turbine monopiles. In: Offshore Site Investigation Geotechnics 8th International Conference Proceedings. Society of Underwater Technology, pp. 142–161. http://dx.doi.org/10.3723/OSIG17.142.

Byrne, B.W., McAdam, R.A., Burd, H.J., Houlsby, G.T., Martin, C.M., Zdravković, L., Taborda, D.M.G., Potts, D.M., Jardine, R.J., Sideri, M., Schroeder, F.C., Gavin, K., Doherty, P., Igoe, D.J.P., Wood, A., Kallehave, D., Gretlund, J.S., 2015. New design methods for large diameter piles under lateral loading for offshore wind applications. Front. Offshore Geotech. III 705–710. http://dx.doi.org/10.1201/b18442-96.

Chen, Y., Ni, P., Han, J., Zhao, W., Jia, P., Zheng, W., 2022. Stress distribution of embedded caisson foundation under lateral load based on the continuum approach. Mar. Georesour. Geotechnol. 40 (11), 1328–1340. http://dx.doi.org/10.1080/1064119X.2021.1992810.

Chortis, G., Askarinejad, A., Prendergast, L.J., Li, Q., Gavin, K., 2020. Influence of scour depth and type on p–y curves for monopiles in sand under monotonic lateral loading in a geotechnical centrifuge. Ocean Eng. 197, 106838. http://dx.doi.org/10.1016/j.oceaneng.2019.106838.

Cox, W.R., Reese, L.C., Grubbs, B.R., 1974. Field testing of laterally loaded piles in sand. In: Offshore Technology Conference. Houston, Texas, http://dx.doi.org/10.4043/2079-MS.

DECC, 2011. UK Renewable Energy Roadmap, Vol. 5. Department of Energy & Climate Change, pp. 293–298. http://dx.doi.org/10.1021/es00108a605.

DNV, 2021. DNVGL-ST-0126 - Support Structures for Wind Turbines. Technical Report July, Det Norske Veritas, Oslo, Norway.

Doherty, P., Gavin, K., 2011. Laterally loaded monopile design for offshore wind farms. Proc. Inst. Civ. Eng. Energy 165 (1), 7–17. http://dx.doi.org/10.1680/ener.11.00003.

Doherty, P., Kirwan, L., Gavin, K., Igoe, D., Tyrrell, S., Ward, D., O'Kelly, B., 2012. Soil properties at the UCD geotechnical research site at Blessington. p. 7.

Dyson, G.J., Randolph, M.F., 2001. Monotonic lateral loading of piles in calcareous sand. J. Geotech. Geoenviron. Eng. 127 (4), 346–352. http://dx.doi.org/10.1061/(ASCE)1090-0241(2001)127:4(346).

Fan, C.C., Long, J.H., 2005. Assessment of existing methods for predicting soil response of laterally loaded piles in sand. Comput. Geotech. 32 (4), 274–289. http://dx.doi.org/10.1016/j.compgeo.2005.02.004.

Fu, D., Zhang, Y., Aamodt, K.K., Yan, Y., 2020. A multi-spring model for monopile analysis in soft clays. Mar. Struct. 72, 102768. http://dx.doi.org/10.1016/j.marstruc.2020.102768.

Gavin, K.G., Igoe, D.J.P., 2021. A field investigation into the mechanisms of pile ageing in sand. Géotechnique 71 (2), 120–131. http://dx.doi.org/10.1680/jgeot.18.P.235.

Gavin, K.G., Igoe, D.J.P., Kirwan, L., 2013. The effect of ageing on the axial capacity of piles in sand. Proc. Inst. Civ. Eng. Geotech. Eng. 166 (2), 122–130. http://dx.doi.org/10.1680/geng.12.00064.

Gavin, K.G., Lehane, B., 2007. Base load – displacement response of piles in sand. Can. Geotech. J. 44 (9), 1053–1063. http://dx.doi.org/10.1139/T07-048.

Gavin, K.G., O'Kelly, B.C., 2007. Effect of friction fatigue on pile capacity in dense sand. J. Geotech. Geoenviron. Eng. 133 (1), 63–71. http://dx.doi.org/10.1061/(ASCE)1090-0241(2007)133:1(63).

Gerolymos, N.A., Gazetas, G., 2005. Winkler model for lateral response of rigid caisson foundations in linear soil. Soil Dyn. Earthq. Eng. 26 (5), 347–361. http://dx.doi.org/10.1016/j.soildyn.2005.12.003.

Gupta, B.K., Basu, D., 2018. Applicability of Timoshenko, Euler–Bernoulli and rigid beam theories in analysis of laterally loaded monopiles and piles. Géotechnique 68 (9), 772–785. http://dx.doi.org/10.1680/jgeot.16.P.244.

Jardine, R.J., Chow, F., Overy, R., Standing, J., 2005. ICP Design Methods for Driven Piles in Sands and Clays. Thomas Telford London.

Jeanjean, P., Zhang, Y., Zakeri, A., Anderson, K.H., Gilbert, R., Senanayake, A.I.M.J., 2011. A framework for monotonic P-y curves in clays.

Kallehave, D., Byrne, B.W., LeBlanc Thilsted, C., Mikkelsen, K.K., 2015. Optimization of monopiles for offshore wind turbines. Phil. Trans. R. Soc. A 373 (2035), 20140100. http://dx.doi.org/10.1098/rsta.2014.0100.

Lam, I.P., 2013. Diameter effects on P-y curves. In: Bittner, R.B., Ellman, A. (Eds.), Deep Marine Foundations: A Perspective on the Design and Construction of Deep Marine Foundations. 16.

Lehane, B.M., Gavin, K.G., 2001. Base resistance of jacked pipe piles in sand. J. Geotech. Geoenviron. Eng. 127 (6), 473–480. http://dx.doi.org/10.1061/(ASCE)1090-0241(2001)127:6(473).

Lehane, B.M., Li, L., Bittar, E.J., 2020a. Cone penetration test-based load-transfer formulations for driven piles in sand. Géotech. Lett. 10 (4), 568–574. http://dx.doi.org/10.1680/jgele.20.00096.

Lehane, B.M., Liu, Z., Bittar, E., Nadim, F., Lacasse, S., Jardine, R.J., Carotenuto, P., Jeanjean, P., Rattley, M., Gavin, K., O'Neill, M.W., 2020b. A new 'unified' CPT-based axial pile capacity design method for driven piles in sand. In: 4th International Symposium on Frontiers in Offshore Geotechnics. American Society of Civil Engineers, Austin, pp. 463–477.

Lehane, B.M., Schneider, A.J., Xu, X., 2005. The UWA-05 method for prediction of axial capacity of driven piles in sand. Front. Offshore Geotech. 683–689. http://dx.doi.org/10.1201/noe0415390637.ch76.

Lehane, B.M., Suryasentana, S., 2014. Verification of numerically derived CPT based P-y curves for piles in sand: 3rd international symposium on cone penetration testing. In: 3rd International Symposium on Cone Penetration Testing, Vol. 1. Omni Press, USA, pp. 1013–1020.

Li, W., Igoe, D., Gavin, K., 2014. Evaluation of CPT-based $p - y$ models for laterally loaded piles in siliceous sand. Géotech. Lett. 4 (2), 110–117. http://dx.doi.org/10.1680/geolett.14.00021.

McAdam, R.A., Byrne, B.W., Houlsby, G.T., Beuckelaers, W.J.A.P., Burd, H.J., Gavin, K.G., Igoe, D.J.P., Jardine, R.J., Martin, C.M., Muir Wood, A., Potts, D.M., Skov Gretlund, J., Taborda, D.M.G., Zdravković, L., 2020. Monotonic laterally loaded pile testing in a dense marine sand at Dunkirk. Géotechnique 70 (11), 986–998. http://dx.doi.org/10.1680/jgeot.18.PISA.004.

Murchinson, J.R., O'Neill, M.W., 1986. Evaluation of P-y relationships in cohesionless soils. Int. J. Rock Mech. Min. Sci. Geomech. Abstr. 23 (3), 109. http://dx.doi.org/10.1016/0148-9062(86)91228-3.

Murphy, G., Igoe, D., Doherty, P., Gavin, K., 2018. 3D FEM approach for laterally loaded monopile design. Comput. Geotech. 100, 76–83. http://dx.doi.org/10.1016/j.compgeo.2018.03.013.

Novello, E., 1999. From static to cyclic P-y data in calcareous sediments. In: Al-Shafei, K. (Ed.), Engineering for Calcareous Sediments. Rotterdam, the Netherlands, pp. 17–24.

O'Neill, M.W., 2001. Side resistance in piles and drilled shafts. J. Geotech. Geoenviron. Eng. 127 (1), 3–16. http://dx.doi.org/10.1061/(ASCE)1090-0241(2001)127:1(3).

O'Neill, M.W., Murchison, J.M., 1983. An Evaluation of Py Relationships in Sands. A Report to the American Petroleum Institute (GT-DF02-83). Technical Report, University of Houston, Houston, Texas.

Paik, K., Salgado, R., Lee, J., Kim, B., 2003. Behavior of open- and closed-ended piles driven into sands. J. Geotech. Geoenviron. Eng. 129 (4), 296–306. http://dx.doi.org/10.1061/(ASCE)1090-0241(2003)129:4(296).

Poulos, H.G., Hull, T., 1989. The role of analytical geomechanics in foundation engineering. In: Kulhawy, F.H. (Ed.), Foundation Engineering: Current Principles and Practices. ASCE, New York, pp. 1578–1606.

Reese, L.C., Cox, W.R., Koop, F.D., 1974. Analysis of laterally loaded piles in sand. In: All Days. OTC, Reston, Virginia, pp. 95–105. http://dx.doi.org/10.4043/2080-MS.

Reese, L.C., Cox, W.R., Koop, F.D., 1975. Field testing and analysis of laterally loaded piles in stiff clay. In: All Days. OTC, Houston, Texas, pp. OTC–2312–MS. http://dx.doi.org/10.4043/2312-MS.

Suryasentana, S.K., Lehane, B.M., 2014. Numerical derivation of CPT-based p–y curves for piles in sand. Géotechnique 64 (3), 186–194. http://dx.doi.org/10.1680/geot.13.P.026.

Suryasentana, S.K., Lehane, B.M., 2016. Updated CPT-based p – y formulation for laterally loaded piles in cohesionless soil under static loading. Géotechnique 66 (6), 445–453. http://dx.doi.org/10.1680/jgeot.14.P.156.

Taborda, D.M.G., Zdravković, L., Potts, D.M., Burd, H.J., Byrne, B.W., Gavin, K.G., Houlsby, G.T., Jardine, R.J., Liu, T., Martin, C.M., McAdam, R.A., 2020. Finite-element modelling of laterally loaded piles in a dense marine sand at dunkirk. Géotechnique 70 (11), 1014–1029. http://dx.doi.org/10.1680/jgeot.18.PISA.006.

Tedesco, J.W., 1999. In: McDougal, W.G., Ross, C.A. (Eds.), Structural Dynamics : Theory and Applications. Addison Wesley Longman, Menlo Park, Calif. ; Harlow.

Thieken, K., Achmus, M., Lemke, K., Terceros, M., 2015. Evaluation of P-y approaches for large-diameter monopiles in sand. Int. J. Offshore Polar Eng. 25 (2), 134–144. http://dx.doi.org/10.17736/ijope.2015.cg09.

Tolooiyan, A., Gavin, K., 2011. Modelling the cone penetration test in sand using cavity expansion and arbitrary Lagrangian Eulerian finite element methods. Comput. Geotech. 38 (4), 482–490. http://dx.doi.org/10.1016/j.compgeo.2011.02.012.

Van Impe, W.F., Wang, S.-T., 2020. The advanced P-y method for analyzing the behaviour of large-diameter monopiles supporting offshore wind turbines. In: McCartney, J., Tomac, I. (Eds.), E3S Web Conf. 205, 12008. http://dx.doi.org/10.1051/e3sconf/202020512008.

Wind Europe, 2021a. Technical Report, pp. 1–39.

Wind Europe, 2021b. Wind Energy in Europe: 2020 Statistics and the Outlook for 2021–2025. Technical Report.

Winkler, E., 1867. Theory of Elasticity and Strength. Dominicus Prague.

Zdravković, L., Jardine, R.J., Taborda, D.M.G., Abadias, D., Burd, H.J., Byrne, B.W., Gavin, K.G., Houlsby, G.T., Igoe, D.J.P., Liu, T., Martin, C.M., McAdam, R.A., Muir Wood, A., Potts, D.M., Skov Gretlund, J., Ushev, E., 2020a. Ground characterisation for PISA pile testing and analysis. Géotechnique 70 (11), 945–960. http://dx.doi.org/10.1680/jgeot.18.PISA.001.

Zdravković, L., Taborda, D.M.G., Potts, D.M., Abadias, D., Burd, H.J., Byrne, B.W., Gavin, K.G., Houlsby, G.T., Jardine, R.J., Martin, C.M., McAdam, R.A., Ushev, E., 2020b. Finite-element modelling of laterally loaded piles in a stiff glacial clay till at Cowden. Géotechnique 70 (11), 999–1013. http://dx.doi.org/10.1680/jgeot.18.PISA.005.

Zhang, Y., Andersen, K., 2019. Soil reaction curves for monopiles in clay. Mar. Struct. 65 (February 2018), 94–113. http://dx.doi.org/10.1016/j.marstruc.2018.12.009.